Contents lists available at ScienceDirect

NeuroImage: Clinical

Motor cortical patterns of upper motor neuron pathology in amyotrophic lateral sclerosis: A 3 T MRI study with iron-sensitive sequences

Graziella Donatelli [a,b], Mauro Costagli [c,d,*], Paolo Cecchi [a,b], Gianmichele Migaleddu [a], Francesca Bianchi [e], Paolo Frumento [f], Gabriele Siciliano [e], Mirco Cosottini [a,g]

[a] Neuroradiology Unit, Azienda Ospedaliero-Universitaria Pisana, Pisa, Italy
[b] Imago7 Research Foundation, Pisa, Italy
[c] Department of Neuroscience, Rehabilitation, Ophthalmology, Genetics, Maternal and Child Sciences (DINOGMI), University of Genova, Genova, Italy
[d] Laboratory of Medical Physics and Magnetic Resonance, IRCCS Stella Maris, Pisa, Italy
[e] Neurology Unit, Department of Clinical and Experimental Medicine, University of Pisa, Pisa, Italy
[f] Department of Political Sciences, University of Pisa, Pisa, Italy
[g] Department of Translational Research and New Technologies in Medicine and Surgery, University of Pisa, Pisa, Italy

ARTICLE INFO

ABSTRACT

Background: Patterns of initiation and propagation of disease in Amyotrophic Lateral Sclerosis (ALS) are still partly unknown. Single or multiple foci of neurodegeneration followed by disease diffusion to contiguous or connected regions have been proposed as mechanisms underlying symptom occurrence. Here, we investigated cortical patterns of upper motor neuron (UMN) pathology in ALS using iron-sensitive MR imaging.
Methods: Signal intensity and magnetic susceptibility of the primary motor cortex (M1), which are associated with clinical UMN burden and neuroinflammation, were assessed in 78 ALS patients using respectively T2*-weighted images and Quantitative Susceptibility Maps. The signal intensity of the whole M1 and each of its functional regions was rated as normal or reduced, and the magnetic susceptibility of each M1 region was measured.
Results: The highest frequencies of T2* hypointensity were found in M1 regions associated with the body sites of symptom onset. Homologous M1 regions were both hypointense in 80–93 % of patients with cortical abnormalities, and magnetic susceptibility values measured in homologous M1 regions were strongly correlated with each other ($\rho = 0.88$; $p < 0.0001$). In some cases, the T2* hypointensity was detectable in two non-contiguous M1 regions but spared the cortex in between.
Conclusions: M1 regions associated with the body site of onset are frequently affected at imaging. The simultaneous involvement of both homologous M1 regions is frequent, followed by that of adjacent regions; the affection of non-contiguous regions, instead, seems rare. This type of cortical involvement suggests the interhemispheric connections as one of the preferential paths for the UMN pathology diffusion in ALS.

1. Introduction

Amyotrophic lateral sclerosis (ALS) is a progressive and clinically heterogeneous (Chiò et al., 2011) neurological disease primarily affecting the voluntary motor system with the degeneration of both cortical and bulbar/spinal motor neurons (respectively upper motor neurons, UMNs, and lower motor neurons, LMNs) (Brooks et al., 2000).

Besides the motor impairment, the frequent occurrence of neuropsychological deficits, which range from mild cognitive or behavioural symptoms to overt frontotemporal dementia, has led to consider ALS as a multi-system disorder (Christidi et al., 2018).

The motor phenotypes of the disease exist in a continuum which extends across a variable mix of UMN and LMN impairment and different body regions of onset (Cosottini et al., 2016; Ravits and La

Spada, 2009; Zoccolella et al., 2006). The clinical onset is typically focal (Fujimura-Kiyono et al., 2011; Körner et al, 2011; Ravits et al., 2007; Ravits and La Spada, 2009; Ravits, 2014; Walhout et al., 2018), with symptoms appearing in one limb or in the orofacial region. Then, the disease gets worse in the region of onset and progresses affecting contiguous and, less frequently, non-contiguous somatic areas (Brooks, 1991; Fujimura-Kiyono et al., 2011; Gargiulo-Monachelli et al., 2012; Ravits and La Spada, 2009; Ravits 2014; Turner et al., 2010; Walhout et al., 2018; Zhenfei et al., 2019) until the respiratory function is supported (Ravits and La Spada, 2009), leading to an extensive involvement of both UMNs and LMNs (Dharmadasa et al., 2020; Sabatelli et al., 2011).

The reason why the disease starts in one body site or another, the linkage between UMN and LMN degeneration and patterns of initiation and spread of pathology across body regions and cortical mantle have not yet been completely elucidated. So far, different theories and clinical scenarios have been reported, including the focal onset followed by propagation to contiguous anatomical regions at both the cortical and spinal levels (Ravits et al., 2007; Ravits and La Spada, 2009; Ravits, 2014), the multiple and non-contiguous foci of disease followed by local propagation (Sekiguchi et al., 2014), and the focal onset followed by disease spread to highly connected contralateral cortical/spinal segments (Brooks, 1991; Walhout et al., 2018).

Patterns of disease onset and progression have been investigated in the past mainly using clinical signs and symptoms (Brooks, 1991; Fujimura-Kiyono et al., 2011; Gargiulo-Monachelli et al., 2012; Körner et al., 2011; Ravits et al., 2007; Turner et al., 2010; Walhout et al., 2018; Zhenfei et al., 2019), often without distinguishing between the contribution of UMNs and LMNs (Brooks, 1991; Fujimura-Kiyono et al., 2011; Gargiulo-Monachelli et al., 2012; Zhenfei et al., 2019). Neurophysiological (Sekiguchi et al., 2014; Zhenfei et al., 2019) and imaging studies (Vázquez-Costa et al., 2018) are, instead, less copious and an MRI study has never been purposely performed for this aim.

Even though clinical data are easily available in large cohorts of ALS patients and neurophysiological indices of neuronal dysfunction seem sensitive to preclinical alterations (Wittstock et al., 2007), magnetic resonance imaging (MRI) could support UMN evaluation. MRI can explore the corticomotoneuronal pathology in a few minutes and provide valuable insights into different and coexisting aspects of neurodegeneration: motor neuron loss and neuroinflammation. Indeed, the T2* hypointensity and the increased magnetic susceptibility of the deep layers of the primary motor cortex (M1) have been suggested as markers of UMN impairment and neuroinflammation in ALS as they correlate with the clinical UMN burden (Cosottini et al., 2016; Costagli et al., 2016) and reflect the degree of microglial activation (Pallebage-Gamarallage et al., 2018) and iron load (Costagli et al., 2016; Kwan et al., 2012).

With these premises, we explored patterns of UMN pathology across M1 using qualitative and quantitative iron-sensitive MRI sequences in a large cohort of ALS patients. First, we investigated the relationship between cortical distribution of T2* hypointensity and body region of symptom onset (aim 1); then, we assessed the frequency of the simultaneous radiological involvement of homologous, adjacent (aim 2) or non-contiguous (aim 3) M1 regions.

2. Material and methods

2.1. Patients

We retrospectively selected all the outpatients of the Neurological Unit of the University Hospital of Pisa with the diagnosis of definite or probable ALS (Brooks et al., 2000) or suspected to have ALS who underwent a 3 T MRI exam of the brain between December 2013 and February 2020. We also took notes of patients who had a follow-up MRI scan. All patients suspected to have ALS received the diagnosis of probable or definite ALS in the follow-up.

Clinical data of patients were retrieved from the Hospital database and included the following information: the body region of symptom onset; the disease severity, assessed with the ALS Functional Rating Scale-Revised (ALSFRS-R; range 0–48 with lower scores reflecting greater disability) (Cedarbaum et al., 1999); the UMN impairment, scored using the UMN-scale (range 0–33 with higher scores reflecting greater impairment) (Cosottini et al., 2016); the disease duration, computed as the number of months from symptom onset to MRI exam; the disease progression rate, calculated according to the formula (48 - ALSFRS-R)/(disease duration) (Walhout et al., 2015).

This study was approved by the local ethics committee and all patients gave their written informed consent to examinations and data processing.

2.2. Analyses employed for each aim

2.2.1. Aim 1: To assess the relationship between cortical distribution of T2* hypointensity and body region of symptom onset,

a) we analysed the frequency distribution of the T2* hypointensity in each pair of homologous M1 regions, namely the paracentral lobules, hand knob and orofacial regions (identified as described in following subsection 2.3.b), separately in patients with lower limb, upper limb and bulbar onset (Fig. 1a).

2.2.2. Aim 2: To assess the simultaneous radiological involvement of homologous and adjacent M1 regions,

b) we identified the pairs of M1 regions more frequently affected at the same time in the same patient. For this purpose, we identified all the combinations without repetition of the six M1 regions (i.e., left and right paracentral lobules, hand knob and orofacial regions) taken in pairs. Then, we computed the percentage of patients with T2* hypointensity in both regions in the subgroup of patients with T2* hypointensity in at least one of them (referred to in the text as "concordance rate of T2* hypointensity"). Finally, we identified the pairs of M1 regions with the highest concordance rate of T2* hypointensity (Fig. 1b);

c) we investigated the symmetry of the cortical T2* hypointensity at visual inspection and measuring the magnetic susceptibility of each region of the motor homunculus (Fig. 1c). Our goal was to demonstrate that, when detectable, homologous M1 regions usually had a similar radiological involvement;

d) we assessed appearance and worsening of the cortical T2* hypointensity over time in patients who had a follow-up MRI scan (Fig. 1d).

The interhemispheric fibres have been supposed to be a conduit for the spread of disease (Eisen, 2009) and, in cases of unilateral limb onset, the contralateral limb has been reported as the preferential second body site to be affected (Walhout et al., 2018). Therefore, we expected that homologous M1 regions were both hypointense in most cases, and that the hypointensity was symmetric or get symmetric over time.

2.2.3. Aim 3: To assess the simultaneous radiological involvement of non-contiguous M1 regions,

e) we identified patients who had T2* hypointensity in two non-contiguous M1 regions of the same hemisphere, namely the paracentral lobule and the orofacial region, but normal signal intensity in the cortex in between, that is the hand knob (Fig. 1e).

We defined the non-contiguous involvement as the simultaneous T2* hypointensity in two non-homologous and non-adjacent M1 regions. Among the non-contiguous patterns of M1 pathology, we included in the analysis only those involving the paracentral lobule and the orofacial region and who did not have signal hypointensity in either the left or the right hand knob in order to rule out a combination of transcallosal and contiguous disease diffusion.

The sequential UMN-related impairment of non-contiguous body areas has been reported in a substantial number of patients (Walhout et al., 2018), therefore we expect that some patients had signal hypointensity in two non-contiguous M1 regions.
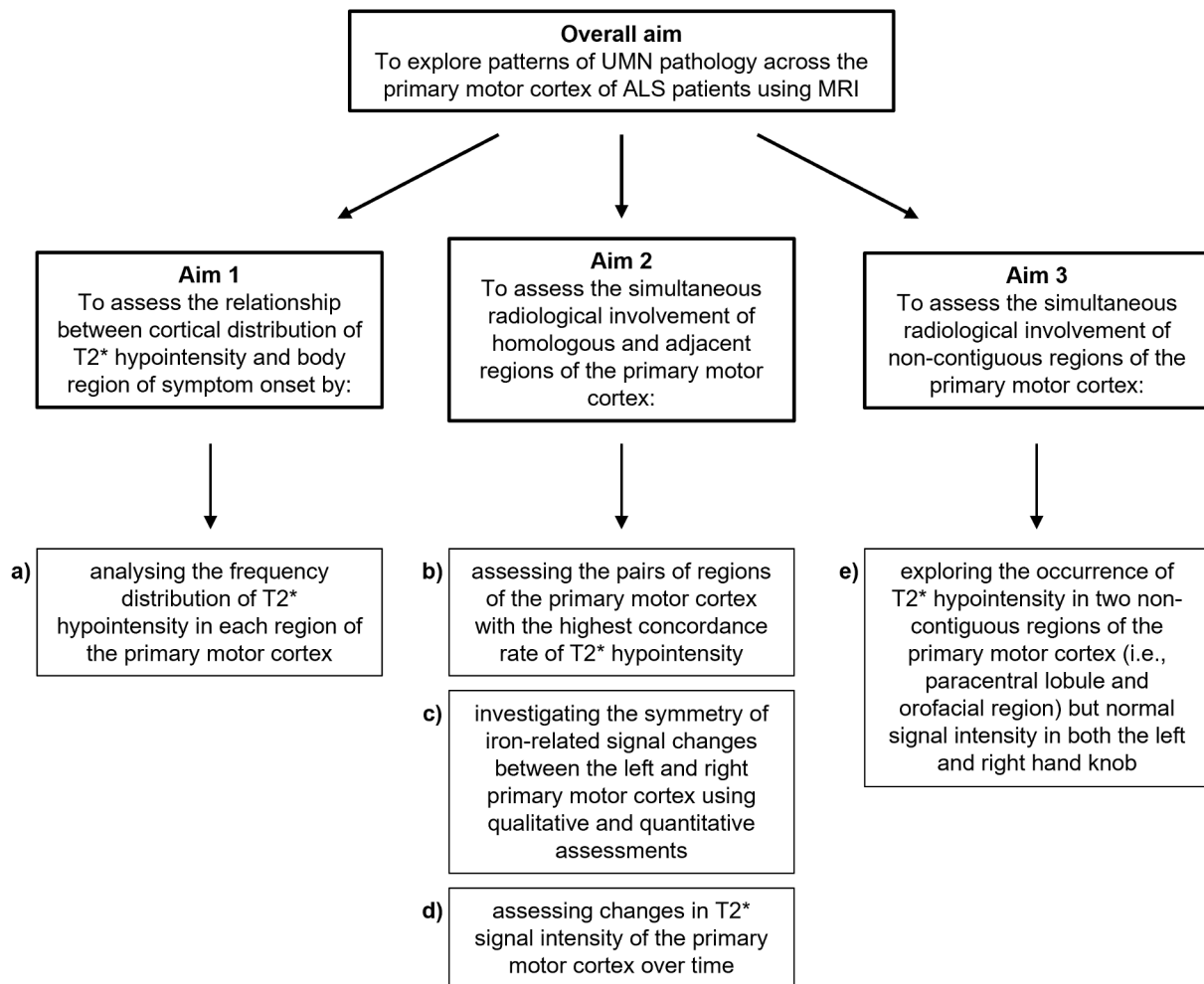
Overall aim
To explore patterns of UMN pathology across the
primary motor cortex of ALS patients using MRI

Aim 1
To assess the relationship
between cortical distribution of
T2* hypointensity and body
region of symptom onset by:

Aim 2
To assess the simultaneous
radiological involvement of
homologous and adjacent
regions of the primary motor
cortex:

Aim 3
To assess the simultaneous
radiological involvement of
non-contiguous regions of the
primary motor cortex:

a) analysing the frequency
distribution of T2*
hypointensity in each region of
the primary motor cortex

b) assessing the pairs of regions
of the primary motor cortex
with the highest concordance
rate of T2* hypointensity

c) investigating the symmetry of
iron-related signal changes
between the left and right
primary motor cortex using
qualitative and quantitative
assessments

d) assessing changes in T2*
signal intensity of the primary
motor cortex over time

e) exploring the occurrence of
T2* hypointensity in two non-
contiguous regions of the
primary motor cortex (i.e.,
paracentral lobule and
orofacial region) but normal
signal intensity in both the left
and right hand knob

Fig. 1. Summary of aims of the study and analyses employed for each aim. UMN, upper motor neuron.

2.3. Imaging acquisition, post-processing and analysis

All MRI exams were performed using a 3 T system (MR750 scanner, GE Healthcare, Milwaukee, WI) equipped with an 8-channel head coil. The acquisition protocol included a 3D T1-weighted image and two 3D gradient multi-echo T2*-weighted sequences.

1) The 3D T1-weighted fast-spoiled gradient echo sequence was used in the processing of T2*-weighted datasets, covered the whole brain and had the following parameters: Time of Repetition, TR = 8.2 ms; Time of Echo, TE = 3.2 ms; Inversion Time = 450 ms; Flip Angle, FA = 12 deg; spatial resolution = $1 \times 1 \times 1$ mm^3, scan duration = 4′33″.

2) The first 3D gradient multi-echo T$_2$*-weighted sequence was used for the visual assessment of M1 (TR = 68.3 ms; TE$_1$:ΔTE:TE$_{10}$ = 13:5.6:63.7 ms; FA = 15 deg; spatial resolution of reconstructed images = $0.39 \times 0.39 \times 1$ mm^3; axial prescription; scan duration = 4′22″). We analysed these images because they are sensitive to iron accumulation within intracortical activated microglia of ALS cases (Kwan et al., 2012), and the iron-related signal hypointensity in M1 has been associated with UMN impairment (Cosottini et al., 2016). Images obtained at the baseline and in the follow-up were inspected in a random order by two neuroradiologists with experience in neuroimaging of ALS. The raters assessed images independently with each other, blinded to clinical information and, when inspecting follow-up scans, also to the results of the analysis of the baseline exam. They focused on the deep layers of M1 because the signal hypointensity locates selectively in this part of the cortex (Kwan et al., 2012; Cosottini et al., 2016; Donatelli et al., 2018). Any disagreement in image interpretation was solved in a consensus reading.

After comparison with the post-central cortex, the signal intensity of the deep layers of M1 was rated as isointense, mildly hypointense or markedly hypointense (Fig. 2) (Donatelli et al., 2019). This evaluation was made separately in each region of the left and right M1, namely paracentral lobules, hand knob and orofacial regions which functionally correspond respectively to lower limbs, upper limbs and face-throat region (Donatelli et al., 2019; Yousry et al., 1997). Both the mild and marked hypointensity were considered abnormal and were referred to as "T2* hypointensity" and "signal change".

Then, the symmetry of the T2* hypointensity between the left and right M1s as well as between the left and right paracentral lobules, hand knob and orofacial regions were assessed in each patient and scored based on the location, degree and length of the hypointense strip as non-symmetric, quite symmetric or highly symmetric (Fig. 3).

3) The second 3D gradient multi-echo T$_2$*-weighted sequence was used to measure the magnetic susceptibility (χ) in each region of the left and right M1. χ is a physical property of the tissue which relates to the presence of diamagnetic and paramagnetic components. It can be measured via Quantitative Susceptibility Mapping, a technique proved to be accurate for iron mapping in grey matter structures (Sun et al., 2015) and already employed to investigate abnormal cortical iron storage in ALS (Acosta-Cabronero et al., 2018; Costagli et al., 2016).

The sequence covered the brain from the vertex to the ponto-bulbar junction and had spatial resolution of $0.94 \times 0.94 \times 1$ mm^3 (TR = 68.1 ms; TE$_1$:ΔTE:TE$_{16}$ = 13:3.4:64.4 ms; FA = 15 deg; axial prescription; scan duration = 8′44″). The magnitude and phase of the complex data
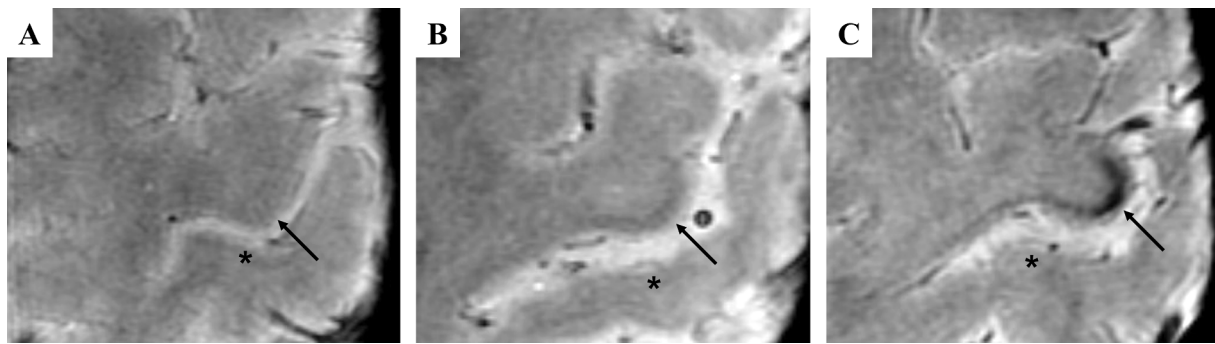
Fig. 2. Examples of the visual score system used to assess the T2* hypointensity of the primary motor cortex. Compared to the post-central cortex (asterisks), the deep layers of the primary motor cortex (arrows) were rated as isointense (A), mildly hypointense (B) or markedly hypointense (C).
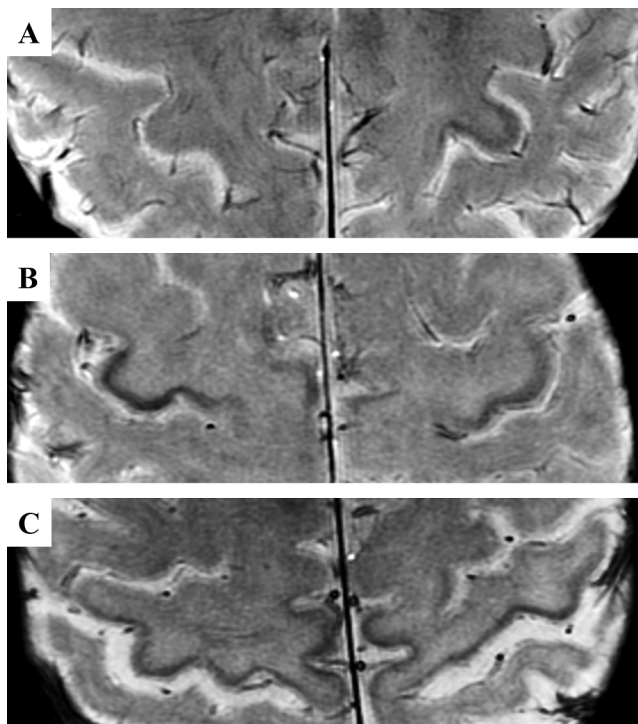

Fig. 3. Examples of the visual score system used to assess the symmetry of T2* hypointensity between the left and right primary motor cortex. The cortical signal change was rated as non-symmetric (A), quite symmetric (B) and highly symmetric (C).

were processed using an established pipeline (Costagli et al., 2016), and both an average T2*-weighted 3D image and a χ map were generated for each dataset.

The 3D T1-weighted image of each patient was brain-extracted using BET (Smith, 2002), part of FSL (FMRIB Software Library package) (Jenkinson et al., 2012). Then, two regions of interest corresponding respectively to the left and right M1 (M1-ROI) were extracted from the Harvard-Oxford Cortical Atlas and, for each patient, placed onto the brain extracted 3D T1-weighted image via nonlinear registration (FSL-FNIRT) (Andersson et al., 2010) and afterward onto the χ map via linear registration (FSL-FLIRT) (Jenkinson et al., 2012).

In order to obtain mean χ values in each region of the motor homunculus (left and right paracentral lobules, hand knob and orofacial regions), the left and right M1 were partitioned into areas associated with each arm and leg and with the face using the BOLD activation maps generated in a healthy subject (female, 36 years old) during appropriate motor tasks. This subject underwent a functional MRI (fMRI) exam,

performed with the 3 T system described above, consisting of five 2D Gradient-Recalled Echo Planar Imaging sequences, one for each of the following motor tasks: flexion–extension of left and right forearms and legs, one limb at a time, and pronunciation of a tongue-twister. fMRI sequences (TR = 3000 ms; TE = 40 ms; FA = 90 deg; spatial resolution = $2 \times 2 \times 4$ mm^3; scan duration = 5′12″) consisted of 28 interleaved slices angled of 30° with respect to the anterior–posterior commissural plane to minimise susceptibility artefacts, repeated over 104 volumes. Each fMRI acquisition consisted in a block-design experiment with task periods of 30 s each alternated to rest periods of 30 s. fMRI data were processed using FEAT tool (Woolrich et al., 2001), part of FSL. The BOLD activation maps were then superimposed on the M1-ROI of each patient via FNIRT registration, and three different regions associated with arm, leg and face were obtained in each hemisphere. Each step of the processing was visually inspected and refined when needed.

Then, for each patient, the mean χ value was computed separately for each M1 region considering only voxels with positive χ values up to 0.125 ppm (Costagli et al., 2016; Donatelli et al., 2019) in order to minimise the presence of tissue other than the cortical grey matter in the ROI.

2.4. Statistical analysis

Continuous data and scores of clinical scales were described by median and interquartile range (IQR). For all pairs of homologous M1 regions of all patients, the relationship between the M1 regions with the highest χ values and the contralateral ones was analysed using the Spearman's correlation coefficient. Statistical analyses were performed using GraphPad Prism 6.

3. Results

Seventy-eight patients met inclusion criteria; their epidemiological and clinical data are reported in Table 1. The clinical onset was unilateral in 84 % of patients with limb onset. Four patients had family history of neurodegenerative diseases.

T2* hypointensity was noted in the M1 of 52 patients (67 %).

3.1. Relationship between cortical distribution of T2* hypointensity and body region of symptom onset

a) In the subgroup of patients with cortical signal change, the T2* hypointensity was recorded more frequently in the M1 area associated with the body region of symptom onset (Table 2): the paracentral lobules were affected in 96 % of patients with lower limb onset, the hand knob in 92 % of patients with upper limb onset and the orofacial regions in all the patients with bulbar onset. Data subgrouped based on the side of symptom onset (left, right or both) and the side of T2* hypointensity (left or right) are reported in **Supplementary Table S1**.

Table 1
Epidemiological and clinical data of ALS patients at the time of the MRI exam.

	ALS patients (n = 78)
Sex (male/female)	41 / 37
Age	65 years (IQR 60–69)
Onset:	
Bulbar	19 (24 %)
Upper limb	20 (26 %): 4 left side, 15 right side, 1 both sides
Lower limb	38 (49 %): 18 left side, 12 right side, 8 both sides
Bulbar + lower limb	1 (1 %)
ALSFRS-R*	42 (IQR 39–44)
UMN score*	7 (IQR 2–11)
Number of patients with UMN impairment in*:	
Oro-facial region	32 (41 %)
Upper limbs†	left: 46 (59 %); right: 51 (65 %)
Lower limbs†	left: 60 (77 %); right: 60 (77 %)
Disease duration (months)	12 (IQR 6–17)
Disease progression rate*	0.50 (IQR 0.32–0.93)
Days between clinical assessment and MRI exam*	25 (IQR 12–62)

ALSFRS-R, Amyotrophic Lateral Sclerosis Functional Rating Scale-Revised; UMN, upper motor neuron.

* Data recorded at the clinical assessment closest to the MRI exam.
† Patients with an UMN score of 1–8 are included.

Table 2
Frequency distribution of T2* hypointensity in each pair of homologous regions of the primary motor cortex (paracentral lobules, hand knob and orofacial regions) according to the body region of symptom onset in patients with cortical signal change.

		Symptom onset		
		Lower limbs	Upper limbs	Bulbar
T2* hypointensity	Paracentral lobules	**96 %**	75 %	65 %
	Hand knob	61 %	**92 %**	59 %
	Orofacial regions	30 %	42 %	**100 %**

The signal intensity of each pair of homologous regions of the primary motor cortex was considered abnormal if T2* hypointensity was noted in at least one of them.

3.2. Assessing the simultaneous radiological involvement of homologous and adjacent M1 regions

b) The homologous M1 regions showed the highest concordance rate of T2* hypointensity, namely the left and right paracentral lobules (concordance rate 93 %), the left and right hand knob (80 %), and the left and right orofacial regions (86 %) (Table 3 and Fig. 4). The average concordance rate of other region pairs was 46 %, and ranged between 30 % and 67 %.

Fourteen patients had only two hypointense M1 regions; all these pairs of M1 regions were homologous.

c) In the subgroup of patients with cortical signal change, the hypointensity between the left and right M1s as well as between the left and right paracentral lobules, hand knob and orofacial regions was highly symmetric or quite symmetric in 83–94 % of cases (Table 4).

Forty-five out of 78 patients had MRI data that enabled to generate a χ map. For each couple of homologous M1 regions, mean χ values in the regions with the higher χ measures correlated significantly with the contralateral ones ($\rho = 0.88$, $p < 0.0001$) (Fig. 5).

d) Six out of 78 patients underwent a second MRI exam including T2*-weighted images for visual analysis. In this subgroup of patients there were 3 males and 3 females, one with bulbar onset and the other five with lower limb onset. The median age at the time of the first MRI

Table 3
Concordance rate of T2* hypointensity in each pair of regions of the primary motor cortex.

	Left orofacial region	Left hand knob	Left paracentral lobule	Right orofacial region	Right hand knob
Right paracentral lobule	42 %	63 %	**93 %**	42 %	67 %
Right hand knob	39 %	**80 %**	61 %	39 %	
Right orofacial region	**86 %**	30 %	37 %		
Left paracentral lobule	37 %	57 %			
Left hand knob	33 %				

For each pair of regions, data reported in the table represent the relative frequencies of patients with T2* hypointensity in both regions among those who had the signal alteration in at least one of them.
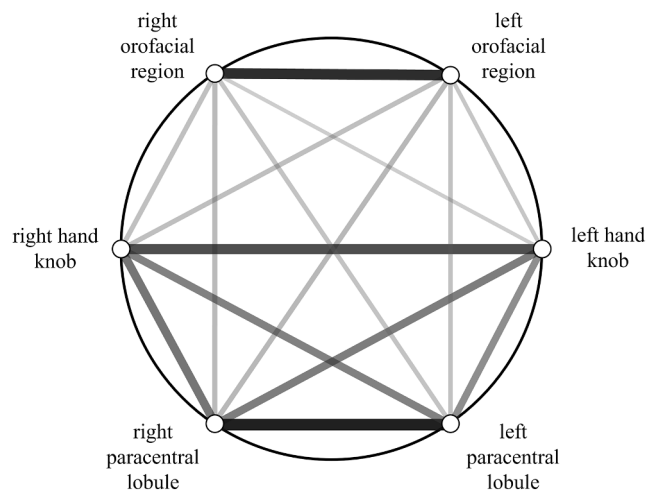

Fig. 4. Graphic representation of the concordance rate of T2* hypointensity in each pair of regions of the primary motor cortex. The darkness and thickness of each line are proportional to the concordance rate.

Table 4
Frequency distribution of the degree of signal hypointensity symmetry between left and right regions of interest in patients with cortical signal change.

	Regions of interest			
	primary motor cortex	paracentral lobules	hand knob	orofacial regions
1) Non-symmetric	5.8 %	11.9 %	17.1 %	17.2 %
2) Quite symmetric	40.4 %	14.3 %	20.0 %	41.4 %
3) Highly symmetric	53.8 %	73.8 %	62.9 %	41.4 %
Total	*100 %*	*100 %*	*100 %*	*100 %*
2 + 3) Quite or highly symmetric	94.2 %	88.1 %	82.9 %	82.8 %

exam was 66 years (IQR 59–69) and the median time between the two MRI exams was 7 months (IQR 6–9). In five of these patients the appearance or worsening of the T2* hypointensity was noted in the follow-up exam, with a tendency towards symmetry of M1 involvement (Figs. 6 and 7).
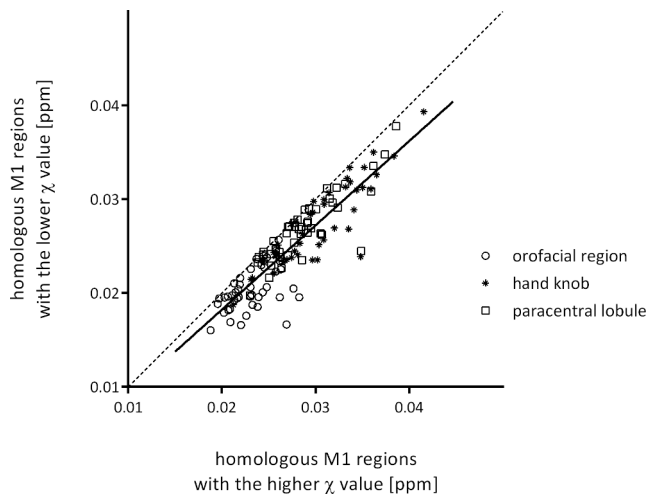
Fig. 5. Graphic representation of the mean magnetic susceptibility values (in ppm) measured in each region of the left and right M1 of ALS patients. For each pair of homologous M1 regions of each patient, the one with the higher susceptibility value is represented in the x-axis, whereas the contralateral one is represented in the y-axis. The dotted line is the bisector of the graph. M1, primary motor cortex.
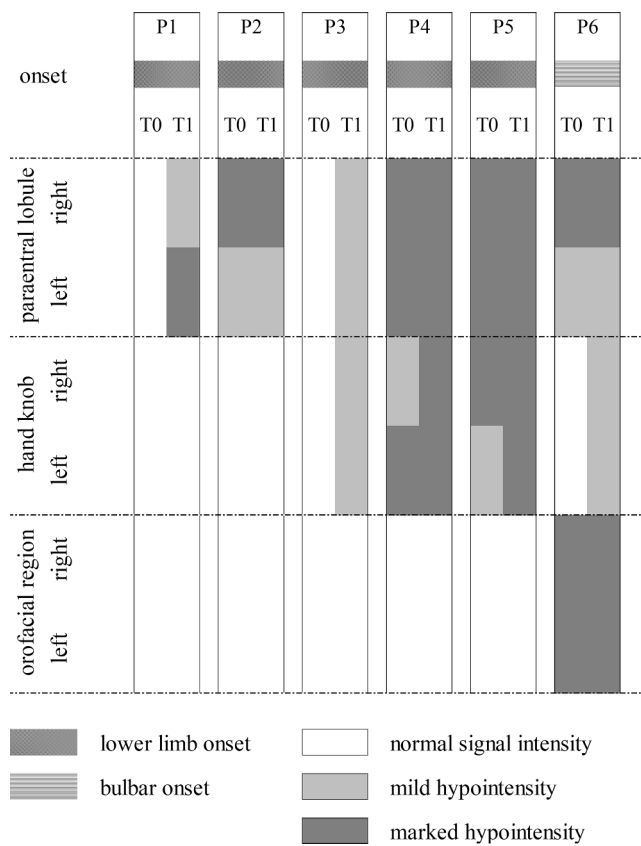

Fig. 6. Greyscale map representing the distribution of normal signal intensity and T2* mild and marked hypointensity along the primary motor cortex of six patients (P1-P6) at the first (T0) and second (T1) MRI exam, based on visual assessment.

3.3. Assessing the simultaneous radiological involvement of non-contiguous M1 regions

e) Four patients had T2* hypointensity in both the paracentral lobule and the orofacial region of the same hemisphere and normal signal intensity in the left and right hand knob (Fig. 8). Two of these patients had bulbar onset and two had lower limb onset.

4. Discussion

In this study we aimed to identify patterns of cortical UMN pathology in a large cohort of ALS patients as revealed by the increased intra-cortical iron accumulation, an indirect marker of corticomotoneuronal degeneration and cortical inflammation.

The mechanisms underlying the progressively increased pool of dysfunctional and injured motor neurons, have not yet been fully elucidated. The main mechanism proposed is the spread of misfolded proteins to neighbouring UMNs through the extracellular matrix, to distant but connected neurons through synapses, and to remote brain regions through the cerebrospinal fluid (Frost and Diamond, 2010; Hasegawa et al., 2011; Kanouchi et al., 2012; Pradat et al., 2015; Smith et al., 2015). It is then reasonable that the mechanism of propagation of pathology could be reflected in the pattern of damage at both the cortical and brainstem/spinal levels and in the resulting clinical picture.

A number of clinical studies have investigated the patterns of disease progression, often without analysing separately symptoms or signs of UMN and LMN impairment (Brooks, 1991; Fujimura-Kiyono et al., 2011; Gargiulo-Monachelli et al., 2012; Zhenfei et al., 2019). Even though the propagation of UMN and LMN pathology might follow the same scheme (Walhout et al., 2018), their separate assessment is a prudent approach as the linkage between cortical and spinal motor neuron degeneration is uncertain. The degeneration, indeed, might start in the UMNs and spread to the LMNs (hypothesis of the anterograde dying-forward degeneration) (Eisen et al., 1992; Hudson and Kiernan, 1988) or vice versa (hypothesis of the retrograde dying-back degeneration) (Chou and Norris, 1993), or might proceed independently at the cortical and bulbar/spinal levels (Attarian et al., 2008; Kiernan and Hudson, 1991; Pamphlett et al., 1995).

Here we focused on the UMN degeneration and analysed cortical signal changes using both qualitative (3D multi-echo T2*-weighted images) and quantitative (Quantitative Susceptibility Mapping) MRI techniques able to reveal and estimate brain iron accumulation (Costagli et al., 2016). Even though T2* hypointensity and high χ values could be associated with a number of paramagnetic substances, non-heme iron is a major susceptibility source in the cortex (Fukunaga et al., 2010) and the cause for cortical susceptibility changes in ALS (Kwan et al., 2012).

Iron is considered an important player in the neurodegenerative process, although it is still a matter of debate whether the misregulation of its metabolism is a cause of the disease and/or its abnormal cortical deposition is the consequence of the neuronal death (Bu et al., 2019). The abnormal storage of iron as ferritin within intracortical activated microglial cells (Kwan et al., 2012) is visible with iron-sensitive MR sequences in ALS patients (Cosottini et al., 2016; Costagli et al., 2016; Donatelli et al., 2018; Kwan et al., 2012). Moreover, cortical micro-gliosis is associated with UMN burden (Cosottini et al., 2016; Costagli et al., 2016) and cortical thinning (Alshikho et al., 2016), therefore T2* hypointensity can be considered an indirect marker of UMN degeneration.

4.1. Relationship between cortical distribution of T2* hypointensity and body region of symptom onset

The first finding of the study is that, when radiologically abnormal, the M1 region more frequently affected was that associated with the site of symptom onset. This is true when the left and right sides are considered together. When data are sub-grouped based also on the side
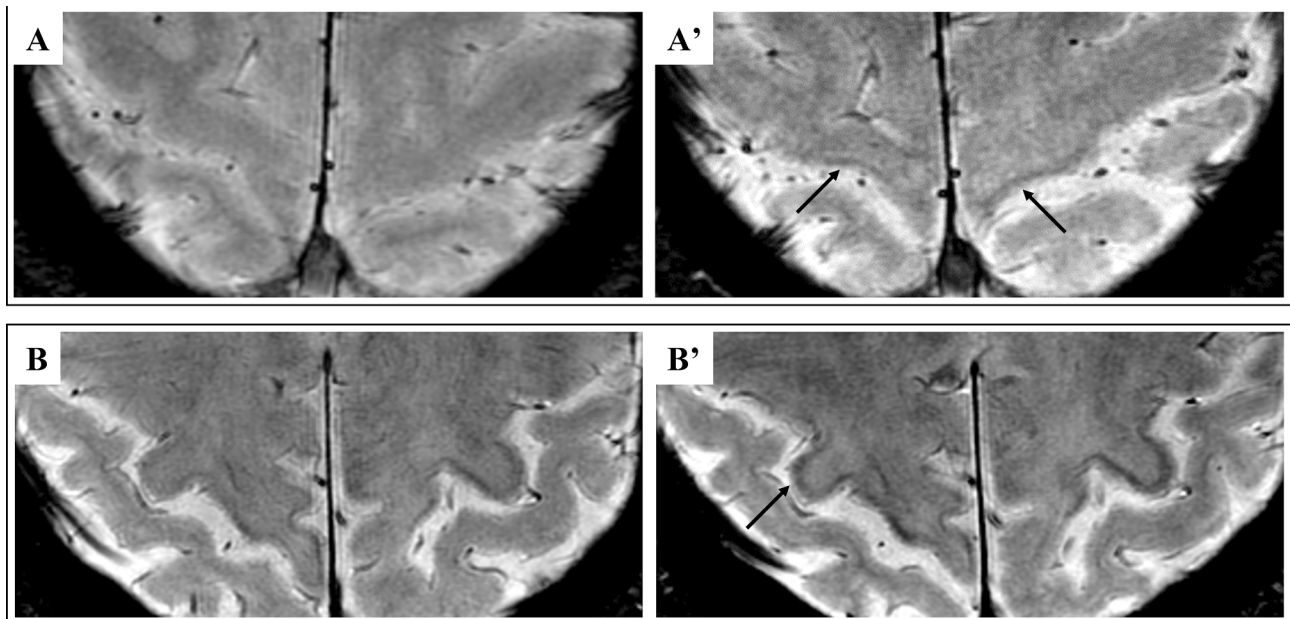
Fig. 7. T2*-weighted images of two patients at the time of the first (A, B) and second (A', B') MRI exam. In the follow-up exams, a cortical hypointense rim appeared in both the paracentral lobules of one patient (upper row) and in the hand knob of the right hemisphere of the other patient (bottom row).
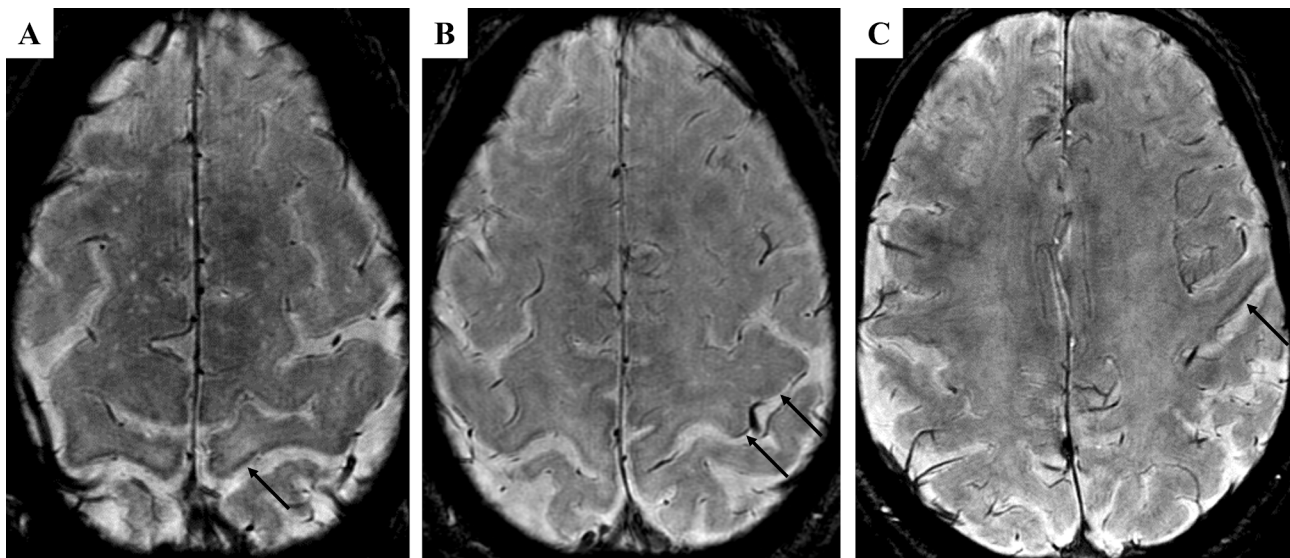

Fig. 8. T2*-weighted images of a patient with T2* hypointensity in the left paracentral lobule (arrow in A) and in the left orofacial region (arrow in C) but with a normal signal intensity in the hand knob (arrows in B).

of symptom onset and T2* hypointensity, instead, groups are too small to reveal an association between side of clinical onset and that of cortical hypointensity.

This result agrees with many (Bede et al., 2013; Dharmadasa et al., 2020; Ravits et al., 2007; Schuster et al., 2013; Schuster et al., 2016; Vázquez-Costa et al., 2018) but not all (Körner et al., 2011) previous studies where abnormal findings at clinical (severity of UMN deficit), neurophysiological (cortical dysfunction) or imaging (cortical atrophy and hypointensity, and subcortical loss of fibre integrity) assessment were shown to match with the body region of symptom onset.

4.2. Assessing the simultaneous radiological involvement of homologous and adjacent M1 regions

The second finding is that in our cohort of patients both qualitative

and quantitative data showed a substantial symmetry of M1 alterations. The homologous M1 regions were those with the highest concordance rate of T2* hypointensity (80–93 %), followed by the couple of adjacent knob-paracentral lobule (57–67 %). In some cases, even though both affected, homologous M1 regions showed a quite symmetric signal hypointensity which appeared even more symmetric in the follow-up scan. Moreover, when only two M1 regions were hypointense, they were homologous in all cases. Based on these results we can gather that the transcallosal propagation of UMN pathology occurs quickly after the appearance of the signal hypointensity, even though the coexistence of multiple and independent foci of neurodegeneration might represent an alternative explanation for this radiological pattern.

Our results are in agreement with the bilateral and often symmetric cortical hypointensity reported by Vázquez-Costa et al. (2018) and the outward spread of disease shown in a previous clinical study. Indeed, in

patients with UMN phenotype and unilateral limb onset, the contralateral limb was reported as the preferential second site to be affected (Walhout et al., 2018). Taken together, our and previous results support the relevance of the corpus callosum in the cortical spread of UMN pathology. While the disease diffusion to adjacent ipsilateral somatic regions could be explained by the contiguous cell-to-cell propagation of the cortical pathology (Ravits and La Spada, 2009; Ravits et al., 2014), the spread to the contralateral limb can be accounted for by propagation along the transcallosal fibres (Walhout et al., 2018).

The role of the corpus callosum as a conduit for the interhemispheric spread of ALS pathology has been suggested some years ago (Eisen, 2009) and is supported by pathological (Cardenas et al., 2017; Smith, 1960; Sugiyama et al., 2013), neurophysiological (van den Bos et al., 2021; Wittstock et al., 2007) and radiological findings (Cardenas et al., 2017; Filippini et al., 2010; Kim et al., 2014; Verstraete et al., 2010). Despite the anatomical distance between homologous M1 regions, it probably acts early in the disease course, as the dysfunction of transcallosal motor fibres is detectable even before the appearance of UMN signs (Wittstock et al., 2007). The most prominent alterations have been found in the posterior midbody and isthmus, where it is crossed by fibres interconnecting the two M1 (Kim et al., 2014). Here, neuronal and non-neuronal alterations have been reported, namely the infiltration of active macrophages/microglia and reactive astrocytes (Cardenas et al., 2017; Sugiyama et al., 2013) together with axonal (Cardenas et al., 2017) and myelin (Cardenas et al., 2017; Smith, 1960) loss.

4.3. Assessing the simultaneous radiological involvement of non-contiguous M1 regions

The third finding is that in a few patients we observed T2* hypointensity in non-contiguous M1 regions, that are the paracentral lobule and the orofacial region of the same hemisphere, without signal abnormalities in the cortex in between. This pattern of MRI alterations could be related to multifocal onset, subsequent and independent foci of neurodegeneration or non-contiguous spread of the disease. However, these patients had bulbar or lower limb onset, therefore we suppose that the involvement of non-contiguous M1 regions was sequential. Other mechanisms, such as the combination of contiguous and transcallosal diffusion of the disease, seem unlikely since both the left and right hand knob were not radiologically affected. This finding, together with the multifocal onset that we recorded in one patient, seems to support the possible occurrence of coexisting pathology in pools of UMNs far from each other. A clinical study including UMN phenotype cases reported a substantial number of patients with sequential involvement of two non-contiguous somatic areas (Walhout et al., 2018). The strict criteria that we used to define the non-contiguous cortical involvement may have led us to underestimate the occurrence of this radiological picture. Additional clinical and neurophysiological data on the UMN impairment in ALS are needed to correctly estimate the incidence of this pattern.

The mechanism responsible for the involvement of non-contiguous M1 regions is still uncertain, but it has been postulated that it may occur as motor neurons become dysfunctional because of their selective vulnerability and/or the remote spread of misfolded proteins through the cerebrospinal fluid (Kanouchi et al., 2012).

4.4. Limitations and future perspectives

This study has some limitations. Firstly, MRI could under-estimate the UMN burden (Donatelli et al., 2018). However, unlike clinical and neurophysiological studies, MRI can provide information about the involvement of the entire M1 in a fast, non-invasive and painless acquisition that can be repeated over time and does not have the confounding influence of LMN degeneration. In particular, MRI could present an added value in cases where the clinical detection of UMN signs is difficult, such as in the orofacial region, or when heavy muscle wasting coexists (Körner et al., 2011; Swash, 2012).

Secondly, the longitudinal analysis in a small sub-group of patients prevents us from drawing definite conclusions on spatial and temporal directionality of the spread of UMN pathology. We can only make inferences based on cross-sectional MRI data of a relatively wide cohort of ALS patients that require longitudinal studies to be confirmed.

Lastly, we employed BOLD activation maps of one healthy volunteer in all ALS patients. This approach relies on the anatomical correspondence between the M1 of the volunteer and those of the patients and avoids doing multiple fMRI acquisitions in suffering patients, but does not account for the inter-individual variability in the cortical localisation of the voluntary motor functions.

To the best of our knowledge, this is the first radiological study which purposely analysed iron-related patterns of M1 involvement in ALS. The results we showed might be useful for sub-grouping patients entering clinical trials (e.g., based on the location of T2* hypointensity in M1, the number of M1 regions involved and the symmetry of the signal change), monitoring disease progression and effectiveness of treatments.

Most observations made in this study were based on the visual inspection of radiological images. This is a fast and practical approach that can be supported by semi-quantitative and automated analysis of presence, location, degree and length of the T2* hypointense strip in M1. For example, the voxel-wise comparison of the two M1 with each other might allow to identify regions of the motor homunculus with an asymmetric signal hypointensity.

As a future perspective, qualitative and quantitative iron-sensitive MR techniques may also be employed to explore pathological iron accumulation in extra-motor brain cortex of ALS patients and possible associations between iron storage and specific neuropsychological deficits (Sheelakumari et al., 2017). Many patients, indeed, experience cognitive or behavioural symptoms and frontotemporal dementia is not an uncommon comorbidity (Christidi et al., 2018). Moreover, frontal and temporal cortical regions showed different patterns of atrophy and iron accumulation across clinical and pathological variants of frontotemporal dementia (Tisdall et al., 2022; Whitwell and Josephs, 2012). Even though cortical regions close to paranasal sinuses cannot be accurately assessed because of susceptibility artefacts due to air-tissue interface, the use of high-resolution images at high magnetic field (3 T) might provide new insight into the pathological correlates of neuropsychological deficits in ALS.

It is worth pointing out that the imaging data of 47 out of 78 ALS patients used in this study were included also in two previous studies (Donatelli et al., 2018; Donatelli et al., 2019).

5. Conclusions

Using qualitative and quantitative MRI techniques, we found that the M1 region more frequently affected was that associated with the site of symptom onset. We also showed that homologous M1 regions are both hypointense in most cases, suggesting that the interhemispheric propagation of the UMN pathology along the transcallosal fibres could be an early path of disease spread at the cortical level. Finally, we showed that simultaneous radiological alterations affecting non-contiguous M1 regions is an apparently less frequent event.

CRediT authorship contribution statement

Graziella Donatelli: Conceptualization, Methodology, Formal analysis, Investigation, Writing – original draft, Writing – review & editing. **Mauro Costagli:** Methodology, Software, Formal analysis, Writing – review & editing. **Paolo Cecchi:** Methodology, Software,

Formal analysis, Writing – review & editing. **Gianmichele Migaleddu:** Investigation, Resources, Writing – review & editing. **Francesca Bianchi:** Investigation, Resources, Writing – review & editing. **Paolo Frumento:** Formal analysis, Writing – review & editing. **Gabriele Siciliano:** Resources, Writing – review & editing. **Mirco Cosottini:** Resources, Supervision, Writing – review & editing.

Declaration of Competing Interest

The authors declare that they have no known competing financial interests or personal relationships that could have appeared to influence the work reported in this paper.

Appendix A. Supplementary data

Supplementary data to this article can be found online at https://doi.org/10.1016/j.nicl.2022.103138.

References

Acosta-Cabronero, J., Machts, J., Schreiber, S., Abdulla, S., Kollewe, K., Petri, S., Spotorno, N., Kaufmann, J., Heinze, H.J., Dengler, R., Vielhaber, S., Nestor, P.J., 2018. Quantitative susceptibility MRI to detect brain iron in amyotrophic lateral sclerosis. Radiology 289 (1), 195–203. https://doi.org/10.1148/radiol.2018180112.

Alshikho, M.J., Zürcher, N.R., Loggia, M.L., Cernasov, P., Chonde, D.B., Izquierdo Garcia, D., Yasek, J.E., Akeju, O., Catana, C., Rosen, B.R., Cudkowicz, M.E., Hooker, J.M., Atassi, N., 2016. Glial activation colocalizes with structural abnormalities in amyotrophic lateral sclerosis. Neurology. 87 (24), 2554–2561. https://doi.org/10.1212/WNL.0000000000003427.

Andersson J.L.R., Jenkinson M., Smith S., 2010. Non-linear registration, aka spatial normalisation. FMRIB technical report TR07JA2 Available: www.fmrib.ox.ac.uk/analysis/techrep.

Attarian, S., Vedel, J.P., Pouget, J., Schmied, A., 2008. Progression of cortical and spinal dysfunctions over time in amyotrophic lateral sclerosis. Muscle Nerve. 37 (3), 364–375. https://doi.org/10.1002/mus.20942.

Bede, P., Bokde, A., Elamin, M., Byrne, S., McLaughlin, R.L., Jordan, N., Hampel, H., Gallagher, L., Lynch, C., Fagan, A.J., Pender, N., Hardiman, O., 2013. Grey matter correlates of clinical variables in amyotrophic lateral sclerosis (ALS): a neuroimaging study of ALS motor phenotype heterogeneity and cortical focality. J. Neurol. Neurosurg. Psychiatry. 84 (7), 766–773. https://doi.org/10.1136/jnnp-2012-302674.

Brooks, B.R., 1991. The role of axonal transport in neurodegenerative disease spread: a meta-analysis of experimental and clinical poliomyelitis compares with amyotrophic lateral sclerosis. Can. J, Neurol, Sci. 18 (3 Suppl), 435–438. https://doi.org/10.1017/s0317167100032625.

Brooks, B.R., Miller, R.G., Swash, M., Munsat, T.L.; World Federation of Neurology Research Group on Motor Neuron Diseases, 2000. El Escorial revisited: revised criteria for the diagnosis of amyotrophic lateral sclerosis. Amyotroph. Lateral. Scler. Other Motor Neuron Disord. 1(5), 293-299. 10.1080/146608200300079536.

Bu, X.L., Xiang, Y., Guo, Y., 2019. The role of iron in amyotrophic lateral sclerosis. Adv Exp. Med, Biol. 1173, 145–152. https://doi.org/10.1007/978-981-13-9589-5_8.

Cardenas, A.M., Sarlls, J.E., Kwan, J.Y., Bageac, D., Gala, Z.S., Danielian, L.E., Ray-Chaudhury, A., Wang, H.W., Miller, K.L., Foxley, S., Jbabdi, S., Welsh, R.C., Floeter, M.K., 2017. Pathology of callosal damage in ALS: An ex-vivo, 7 T diffusion tensor MRI study. Neuroimage Clin. 15, 200–208. https://doi.org/10.1016/j.nicl.2017.04.024.

Cedarbaum, J.M., Stambler, N., Malta, E., Fuller, C., Hilt, D., Thurmond, B., Nakanishi, A., 1999. The ALSFRS-R: a revised ALS functional rating scale that incorporates assessments of respiratory function. BDNF ALS Study Group (Phase III). J. Neurol. Sci. 169 (1–2), 13–21. https://doi.org/10.1016/s0022-510x(99)00210-5.

Chiò, A., Calvo, A., Moglia, C., Mazzini, L., Mora, G.; PARALS study group, 2011. Phenotypic heterogeneity of amyotrophic lateral sclerosis: a population based study. J. Neurol. Neurosurg. Psychiatry. 82 (7), 740-746. 10.1136/jnnp.2010.235952.

Chou, S.M., Norris, F.H., 1993. Amyotrophic lateral sclerosis: lower motor neuron disease spreading to upper motor neurons. Muscle Nerve. 16 (8), 864–869. https://doi.org/10.1002/mus.880160810.

Christidi, F., Karavasilis, E., Rentzos, M., Kelekis, N., Evdokimidis, I., Bede, P., 2018. Clinical and radiological markers of extra-motor deficits in amyotrophic lateral sclerosis. Front. Neurol. 9, 1005. https://doi.org/10.3389/fneur.2018.01005.

Cosottini, M., Donatelli, G., Costagli, M., Caldarazzo Ienco, E., Frosini, D., Pesaresi, I., Biagi, L., Siciliano, G., Tosetti, M., 2016. High-resolution 7T MR imaging of the motor cortex in amyotrophic lateral sclerosis. AJNR Am. J. Neuroradiol. 37 (3), 455–461. https://doi.org/10.3174/ajnr.A4562.

Costagli, M., Donatelli, G., Biagi, L., Caldarazzo Ienco, E., Siciliano, G., Tosetti, M., Cosottini, M., 2016. Magnetic susceptibility in the deep layers of the primary motor cortex in Amyotrophic Lateral Sclerosis. Neuroimage Clin. 12, 965–969. https://doi.org/10.1016/j.nicl.2016.04.011.

Dharmadasa, T., Matamala, J.M., Howells, J., Vucic, S., Kiernan, M.C., 2020. Early focality and spread of cortical dysfunction in amyotrophic lateral sclerosis: A

regional study across the motor cortices. Clin. Neurophysiol. 131 (4), 958–966. https://doi.org/10.1016/j.clinph.2019.11.057.

Donatelli, G., Retico, A., Caldarazzo Ienco, E., Cecchi, P., Costagli, M., Frosini, D., Biagi, L., Tosetti, M., Siciliano, G., Cosottini, M., 2018. Semiautomated evaluation of the primary motor cortex in patients with amyotrophic lateral sclerosis at 3T. AJNR Am. J. Neuroradiol. 39 (1), 63–69. https://doi.org/10.3174/ajnr.A5423.

Donatelli, G., Caldarazzo Ienco, E., Costagli, M., Migaleddu, G., Cecchi, P., Siciliano, G., Cosottini, M., 2019. MRI cortical feature of bulbar impairment in patients with amyotrophic lateral sclerosis. Neuroimage Clin. 24, 101934 https://doi.org/10.1016/j.nicl.2019.101934.

Eisen, A., 2009. Amyotrophic lateral sclerosis-evolutionary and other perspectives. Muscle Nerve. 40 (2), 297–304. https://doi.org/10.1002/mus.21404.

Eisen, A., Kim, S., Pant, B., 1992. Amyotrophic lateral sclerosis (ALS): a phylogenetic disease of the corticomotoneuron? Muscle Nerve. 15 (2), 219–224. https://doi.org/10.1002/mus.880150215.

Filippini, N., Douaud, G., Mackay, C.E., Knight, S., Talbot, K., Turner, M.R., 2010. Corpus callosum involvement is a consistent feature of amyotrophic lateral sclerosis. Neurology. 75 (18), 1645–1652. https://doi.org/10.1212/WNL.0b013e3181fb84d1.

Frost, B., Diamond, M.I., 2010. Prion-like mechanisms in neurodegenerative diseases. Nat. Rev. Neurosci. 11 (3), 155–159. https://doi.org/10.1038/nrn2786.

Fujimura-Kiyono, C., Kimura, F., Ishida, S., Nakajima, H., Hosokawa, T., Sugino, M., Hanafusa, T., 2011. Onset and spreading patterns of lower motor neuron involvements predict survival in sporadic amyotrophic lateral sclerosis. J. Neurol. Neurosurg. Psychiatry. 82 (11), 1244–1249. https://doi.org/10.1136/jnnp-2011-300141.

Fukunaga, M., Li, T.Q., van Gelderen, P., de Zwart, J.A., Shmueli, K., Yao, B., Lee, J., Maric, D., Aronova, M.A., Zhang, G., Leapman, R.D., Schenck, J.F., Merkle, H., Duyn, J.H., 2010. Layer-specific variation of iron content in cerebral cortex as a source of MRI contrast. Proc. Natl. Acad. Sci. U. S. A. 107 (8), 3834–3839. https://doi.org/10.1073/pnas.0911177107.

Gargiulo-Monachelli, G.M., Janota, F., Bettini, M., Shoesmith, C.L., Strong, M.J., Sica, R. E., 2012. Regional spread pattern predicts survival in patients with sporadic amyotrophic lateral sclerosis. Eur. J. Neurol. 19 (6), 834–841. https://doi.org/10.1111/j.1468-1331.2011.03616.x.

Hasegawa, M., Nonaka, T., Tsuji, H., Tamaoka, A., Yamashita, M., Kametani, F., Yoshida, M., Arai, T., Akiyama, H., 2011. Molecular dissection of TDP-43 proteinopathies. J. Mol. Neurosci. 45 (3), 480–485. https://doi.org/10.1007/s12031-011-9571-x.

Hudson, A.J., Kiernan, J.N., 1988. Preservation of certain voluntary muscles in motoneurone disease. Lancet 1 (8586), 652–653. https://doi.org/10.1016/s0140-6736(88)91455-9.

Jenkinson, M., Beckmann, C.F., Behrens, T.E., Woolrich, M.W., Smith, S.M., 2012. FSL. NeuroImage 62 (2), 782–790. https://doi.org/10.1016/j.neuroimage.2011.09.015.

Kanouchi, T., Ohkubo, T., Yokota, T., 2012. Can regional spreading of amyotrophic lateral sclerosis motor symptoms be explained by prion-like propagation? J. Neurol. Neurosurg. Psychiatry. 83 (7), 739–745. https://doi.org/10.1136/jnnp-2011-301826.

Kiernan, J.A., Hudson, A.J., 1991. Changes in sizes of cortical and lower motor neurons in amyotrophic lateral sclerosis. Brain. 114 (Pt 2), 843–853. https://doi.org/10.1093/brain/114.2.843.

Kim, J.E., Oh, J.S., Sung, J.J., Lee, K.W., Song, I.C., Hong, Y.H., 2014. Diffusion tensor tractography analysis of the corpus callosum fibers in amyotrophic lateral sclerosis. J. Clin. Neurol. 10 (3), 249–256. https://doi.org/10.3988/jcn.2014.10.3.249.

Körner, S., Kollewe, K., Fahlbusch, M., Zapf, A., Dengler, R., Krampfl, K., Petri, S., 2011. Onset and spreading patterns of upper and lower motor neuron symptoms in amyotrophic lateral sclerosis. Muscle Nerve. 43 (5), 636–642. https://doi.org/10.1002/mus.21936.

Kwan, J.Y., Jeong, S.Y., Van Gelderen, P., Deng, H.X., Quezado, M.M., Danielian, L.E., Butman, J.A., Chen, L., Bayat, E., Russell, J., Siddique, T., Duyn, J.H., Rouault, T.A., Floeter, M.K., 2012. Iron accumulation in deep cortical layers accounts for MRI signal abnormalities in ALS: correlating 7 tesla MRI and pathology. PLoS ONE 7 (4), e35241.

Pallebage-Gamarallage, M., Foxley, S., Menke, R.A.L., Huszar, I.N., Jenkinson, M., Tendler, B.C., Wang, C., Jbabdi, S., Turner, M.R., Miller, K.L., Ansorge, O., 2018. Dissecting the pathobiology of altered MRI signal in amyotrophic lateral sclerosis: A post mortem whole brain sampling strategy for the integration of ultra-high-field MRI and quantitative neuropathology. BMC Neurosci. 19 (1), 11. https://doi.org/10.1186/s12868-018-0416-1.

Pamphlett, R., Kril, J., Hng, T.M., 1995. Motor neuron disease: a primary disorder of corticomotoneurons? Muscle Nerve. 18 (3), 314–318. https://doi.org/10.1002/mus.880180308.

Pradat, P.F., Kabashi, E., Desnuelle, C., 2015. Deciphering spreading mechanisms in amyotrophic lateral sclerosis: clinical evidence and potential molecular processes. Curr. Opin. Neurol. 28 (5), 455–461. https://doi.org/10.1097/WCO.0000000000000239.

Ravits, J.M., La Spada, A.R., 2009. ALS motor phenotype heterogeneity, focality, and spread: deconstructing motor neuron degeneration. Neurology. 73 (10), 805–811. https://doi.org/10.1212/WNL.0b013e3181b6bbbd.

Ravits, J., Paul, P., Jorg, C., 2007. Focality of upper and lower motor neuron degeneration at the clinical onset of ALS. Neurology. 68 (19), 1571–1575. https://doi.org/10.1212/01.wnl.0000260965.20021.47.

Ravits, J., 2014. Focality, stochasticity and neuroanatomic propagation in ALS pathogenesis. Exp. Neurol. 262 Pt B, 121-126. 10.1016/j.expneurol.2014.07.021.

Sabatelli, M., Zollino, M., Luigetti, M., Grande, A.D., Lattante, S., Marangi, G., Monaco, M.L., Madia, F., Meleo, E., Bisogni, G., Conte, A., 2011. Uncovering amyotrophic lateral sclerosis phenotypes: clinical features and long-term follow-up

of upper motor neuron-dominant ALS. Amyotroph. Lateral Scler. 12 (4), 278–282. https://doi.org/10.3109/17482968.2011.580849.

Schuster, C., Kasper, E., Machts, J., Bittner, D., Kaufmann, J., Benecke, R., Teipel, S., Vielhaber, S., Prudlo, J., 2013. Focal thinning of the motor cortex mirrors clinical features of amyotrophic lateral sclerosis and their phenotypes: a neuroimaging study. J. Neurol. 260 (11), 2856–2864. https://doi.org/10.1007/s00415-013-7083-z.

Schuster, C., Elamin, M., Hardiman, O., Bede, P., 2016. The segmental diffusivity profile of amyotrophic lateral sclerosis associated white matter degeneration. Eur. J. Neurol. 23 (8), 1361–1371. https://doi.org/10.1111/ene.13038.

Sekiguchi, T., Kanouchi, T., Shibuya, K., Noto, Y., Yagi, Y., Inaba, A., Abe, K., Misawa, S., Orimo, S., Kobayashi, T., Kamata, T., Nakagawa, M., Kuwabara, S., Mizusawa, H., Yokota, T., 2014. Spreading of amyotrophic lateral sclerosis lesions–multifocal hits and local propagation? J. Neurol. Neurosurg. Psychiatry. 85 (1), 85–91. https://doi.org/10.1136/jnnp-2013-305617.

Sheelakumari, R., Kesavadas, C., Varghese, T., Sreedharan, R.M., Thomas, B., Verghese, J., et al., 2017. Assessment of Iron Deposition in the Brain in Frontotemporal Dementia and Its Correlation with Behavioral Traits. AJNR Am. J. Neuroradiol. 38 (10), 1953–1958. https://doi.org/10.3174/ajnr.A5339.

Smith, M.C., 1960. Nerve fibre degeneration in the brain in amyotrophic lateral sclerosis. J. Neurol. Neurosurg. Psychiatry. 23 (4), 269–282. https://doi.org/10.1136/jnnp.23.4.269.

Smith, S.M., 2002. Fast robust automated brain extraction. Hum. Brain Mapp. 17 (3), 143–155. https://doi.org/10.1002/hbm.10062.

Smith, R., Myers, K., Ravits, J., Bowser, R., 2015. Amyotrophic lateral sclerosis: Is the spinal fluid pathway involved in seeding and spread? Med. Hypotheses. 85 (5), 576–583. https://doi.org/10.1016/j.mehy.2015.07.014.

Sugiyama, M., Takao, M., Hatsuta, H., Funabe, S., Ito, S., Obi, T., Tanaka, F., Kuroiwa, Y., Murayama, S., 2013. Increased number of astrocytes and macrophages/microglial cells in the corpus callosum in amyotrophic lateral sclerosis. Neuropathology. 33 (6), 591–599. https://doi.org/10.1111/neup.12027.

Sun, H., Walsh, A.J., Lebel, R.M., Blevins, G., Catz, I., Lu, J.Q., Johnson, E.S., Emery, D.J., Warren, K.G., Wilman, A.H., 2015. Validation of quantitative susceptibility mapping with Perls' iron staining for subcortical gray matter. Neuroimage 105, 486–492. https://doi.org/10.1016/j.neuroimage.2014.11.010.

Swash, M., 2012. Why are upper motor neuron signs difficult to elicit in amyotrophic lateral sclerosis? J. Neurol. Neurosurg. Psychiatry. 83 (6), 659–662. https://doi.org/10.1136/jnnp-2012-302315.

Tisdall, M.D., Ohm, D.T., Lobrovich, R., Das, S.R., Mizsei, G., Prabhakaran, K., et al., 2022. Ex vivo MRI and histopathology detect novel iron-rich cortical inflammation in frontotemporal lobar degeneration with tau versus TDP-43 pathology. Neuroimage Clin. 33, 102913 https://doi.org/10.1016/j.nicl.2021.102913.

Turner, M.R., Brockington, A., Scaber, J., Hollinger, H., Marsden, R., Shaw, P.J., Talbot, K., 2010. Pattern of spread and prognosis in lower limb-onset ALS.

Amyotroph. Lateral. Scler. 11 (4), 369–373. https://doi.org/10.3109/17482960903420140.

van den Bos, M.A.J., Higashihara, M., Geevasinga, N., Menon, P., Kiernan, M.C., Vucic, S., 2021. Pathophysiological associations of transcallosal dysfunction in ALS. Eur. J. Neurol. 28 (4), 1172–1180. https://doi.org/10.1111/ene.14653.

Vázquez-Costa, J.F., Mazón, M., Carreres-Polo, J., Hervás, D., Pérez-Tur, J., Martí-Bonmatí, L., Sevilla, T., 2018. Brain signal intensity changes as biomarkers in amyotrophic lateral sclerosis. Acta Neurol. Scand. 137 (2), 262–271. https://doi.org/10.1111/ane.12863.

Verstraete, E., van den Heuvel, M.P., Veldink, J.H., Blanken, N., Mandl, R.C., Hulshoff Pol, H.E., van den Berg, L.H., 2010. Motor network degeneration in amyotrophic lateral sclerosis: a structural and functional connectivity study. PLoS ONE 5 (10), e13664.

Walhout, R., Westeneng, H.J., Verstraete, E., Hendrikse, J., Veldink, J.H., van den Heuvel, M.P., van den Berg, L.H., 2015. Cortical thickness in ALS: towards a marker for upper motor neuron involvement. J. Neurol. Neurosurg. Psychiatry. 86 (3), 288–294. https://doi.org/10.1136/jnnp-2013-306839.

Walhout, R., Verstraete, E., van den Heuvel, M.P., Veldink, J.H., van den Berg, L.H., 2018. Patterns of symptom development in patients with motor neuron disease. Amyotroph. Lateral. Scler. Frontotemporal Degener. 19 (1–2), 21–28. https://doi.org/10.1080/21678421.2017.1386688.

Whitwell, J.L., Josephs, K.A., 2012. Recent advances in the imaging of frontotemporal dementia. Curr. Neurol. Neurosci. Rep. 12 (6), 715–723. https://doi.org/10.1007/s11910-012-0317-0.

Wittstock, M., Wolters, A., Benecke, R., 2007. Transcallosal inhibition in amyotrophic lateral sclerosis. Clin. Neurophysiol. 118 (2), 301–307. https://doi.org/10.1016/j.clinph.2006.09.026.

Woolrich, M.W., Ripley, B.D., Brady, M., Smith, S.M., 2001. Temporal Autocorrelation in Univariate Linear Modeling of FMRI Data. NeuroImage 14 (6), 1370–1386. https://doi.org/10.1006/nimg.2001.0931.

Yousry, T.A., Schmid, U.D., Alkadhi, H., Schmidt, D., Peraud, A., Buettner, A., Winkler, P., 1997. Localization of the motor hand area to a knob on the precentral gyrus. A new landmark. Brain. 120 (Pt 1), 141–157. https://doi.org/10.1093/brain/120.1.141.

Zhenfei, L., Shiru, D., Xiaomeng, Z., Cuifang, C., Yaling, L., 2019. Discontiguous or Contiguous Spread Patterns Affect the Functional Staging in Patients With Sporadic Amyotrophic Lateral Sclerosis. Front. Neurol. 10, 523. https://doi.org/10.3389/fneur.2019.00523.

Zoccolella, S., Beghi, E., Palagano, G., Fraddosio, A., Samarelli, V., Lamberti, P., Lepore, V., Serlenga, L., Logroscino, G.; SLAP registry, 2006. Signs and symptoms at diagnosis of amyotrophic lateral sclerosis: a population-based study in southern Italy. Eur. J. Neurol. 13 (7), 789-792. 10.1111/j.1468-1331.2006.01384.x.